

The activity-weight duality in feed forward neural networks: The geometric determinants of generalization

Yu Feng^{1,2} and Yuhai Tu¹

¹IBM T. J. Watson Research Center, NY 10598

²Department of Physics, Duke University, Durham, NC 27710

(March 23, 2022)

Abstract

One of the fundamental problems in machine learning is generalization. In neural network models with a large number of weights (parameters), many solutions can be found to fit the training data equally well. The key question is which solution can describe testing data not in the training set. Here, we report the discovery of an exact duality (equivalence) between changes in activities in a given layer of neurons and changes in weights that connect to the next layer of neurons in a densely connected layer in any feed forward neural network. The activity-weight (A-W) duality allows us to map variations in inputs (data) to variations of the corresponding dual weights. By using this mapping, we show that the generalization loss can be decomposed into a sum of contributions from different eigen-directions of the Hessian matrix of the loss function at the solution in weight space. The contribution from a given eigen-direction is the product of two geometric factors (determinants): the sharpness of the loss landscape and the standard deviation of the dual weights, which is found to scale with the weight norm of the solution. Our results provide an unified framework, which we used to reveal how different regularization schemes (weight decay, stochastic gradient descent with different batch sizes and learning rates, dropout), training data size, and labeling noise affect generalization performance by controlling either one or both of these two geometric determinants for generalization. These insights can be used to guide development of algorithms for finding more generalizable solutions in overparametrized neural networks.

1 Introduction

Generalization is one of the most important problems in machine learning. This problem becomes more pressing given the recent advances in deep learning neural networks (DLNN) [1,2], which have enjoyed a long string of tremendous successes in achieving human level performance in image recognition [3], machine translation [4], games [5], and even solving longstanding grand challenge scientific problems such as protein folding [6]. Endowed with an overwhelming number of parameters, these structured feed forward neural network models can be trained efficiently by using gradient descent down a global loss function to fit the training data. However, given the large number of parameters in DLNN, there are many different solutions that can fit the training data perfectly. The quality of a solution is determined by its generalizability, i.e., how well the solution fits a test data set that the neural network has not seen before [7].

There has been much recent work on generalization in DLNN based on various theoretically and empirically motivated complexity measures (VC-dimension, norm of parameters, sharpness, path norms, etc.) of the solution, see Jiang et al [8] for a recent comprehensive review on the subject and the references therein. However, despite empirical evidence for a strong correlation between sharpness-based measures and generalization [9], the other (theoretically motivated) measures such as the norm-based measures do not serve as robust indicators for generalization by themselves [8]. Even in the case of the more promising sharpness-based measures, we do not understand exactly why and how they work, and there are work challenging the usefulness of using loss landscape sharpness alone for determining generalization [10]. Indeed, a deep understanding of generalization in DLNN still remains elusive.

Here, we tackle the generalization problem by using a different approach. The general motivation is that if there exists an equivalence (duality) between a change of the input between a training data (\mathbf{x}) and a testing data (\mathbf{x}') and a corresponding change of the weights from the solution (\mathbf{w}) to a new weight (\mathbf{w}'), we can then use this duality to map a distribution in the input space to a distribution in the weight space, where we can evaluate the generalization loss. Remarkably, we find an infinite family of such exact equivalence (duality) relations between changes in activities and weights in any densely connected layer in feed forward neural networks. By using the “minimal” duality relation with the smallest weight change, we decompose the generalization loss to contributions from different eigen-directions of the Hessian matrix of the loss function at the solution in the weight space. The form of these contributions reveals two determining factors (determinants) for generalization – one is governed by the sharpness of the loss landscape and the other corresponds

to the norm of the solution weighted by the covariance of the relative differences between the training and testing data set. By using this exact decomposition, we show how various implicit and explicit regularization schemes improve generalization by affecting one or both of these determinants.

2 The activity-weight duality in feed-forward neural networks

In a neural network, the loss function $l(\mathbf{w}, \mathbf{x})$ depends on both the input data (\mathbf{x}) and parameters of the model given by the weights (\mathbf{w}) in the network. The weights are learnt by minimizing the overall loss function averaged over a set of training samples. Given the over-parametrization nature of deep nets, the training loss can be very small or near zero; however, the generalization performance of the model is determined by the loss $l(\mathbf{w}, \mathbf{x}')$ for testing sample \mathbf{x}' , which is different from \mathbf{x} even though they belong to the same distribution. To understand the difference between $l(\mathbf{w}, \mathbf{x})$ and $l(\mathbf{w}, \mathbf{x}')$, we look for a possible data-parameter duality relation:

$$l(\mathbf{w}, \mathbf{x}') = l(\mathbf{w}', \mathbf{x}), \quad (1)$$

which means that in terms of the loss function a change from \mathbf{x} to \mathbf{x}' with fixed parameters \mathbf{w} is equivalent to changing the parameters from \mathbf{w} to \mathbf{w}' without changing the data (see Fig. 1A for an illustration). Here, \mathbf{w}' is called a dual weight corresponding to \mathbf{x}' .

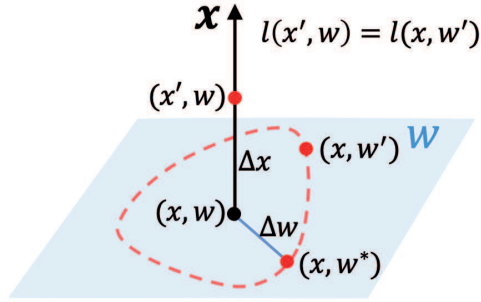
In a feed-forward neural network, the activity of a neuron j in a hidden layer (h_2) is determined by the pre-activation factor $a_j = \sum_i w_{ij} x_i$ where x_i is the activity of neuron- i in the previous layer (h_1) in the network (the input layer is considered as the first layer of the network). Since the loss function in the feed-forward neural network only depends on the outputs (activities) of neurons in a given layer h_j : $x_j = \phi(a_j)$ with $\phi(\cdot)$ the activation function, and the weights beyond the current layer, the duality relation Eq. 1 can be satisfied if the dual weights \mathbf{w}' are chosen to keep a_j unchanged:

$$\sum_{i=1}^{L_1} w'_{ij} x_i = \sum_{i=1}^{L_1} w_{ij} x'_i, \quad j = 1, 2, \dots, L_2 \quad (2)$$

where L_1 and L_2 are the number of neurons in layer h_1 and h_2 , respectively.

In a densely connected layer such as a fully connected layer (FCL), the total number of weights ($M = L_1 L_2$) is larger than the number of neurons (L_2); therefore

A. The activity-weight (A-W) duality



B. The minimal A-W duality

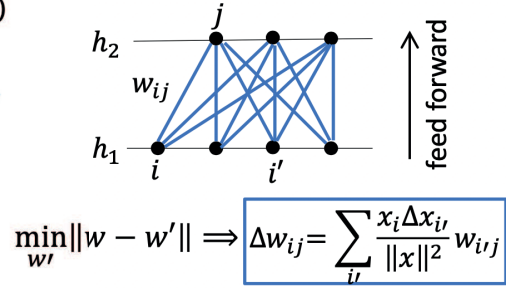


Figure 1: The activity-weight duality. (A) Illustration of the duality relation. The activity and weight are represented by the vertical direction and the horizontal plane (shaded blue), respectively. The loss for a new activity \mathbf{x}' at the original weight \mathbf{w} (red dot on the vertical axis) is the same as the loss at the original activity (\mathbf{x}) at a new weight \mathbf{w}' , which can be any point on the dotted red line in the weight(\mathbf{w})-plane. (B) Between two densely connected layers (h_1 and h_2) in a feed-forward network, changes of weights ($\Delta\mathbf{w}$) for the duality relation with the minimum $\|\Delta\mathbf{w}\|_2$ are given explicitly by the original weights (\mathbf{w}), the original activity (\mathbf{x}) and the changes in activity ($\Delta\mathbf{x}$) in the input layer (h_1).

there are an infinite number of solutions for \mathbf{w}' that satisfies the duality condition (Eq. 2). Here, we focus on the “minimal” duality solution \mathbf{w}^* that is the closest to the original weights \mathbf{w} (Note that we represent the weights as a M -dimensional vector). The minimal duality solution \mathbf{w}^* can be obtained by minimizing $\|\mathbf{w}' - \mathbf{w}\|^2$ under the constraints given by Eq. 2. This problem can be solved exactly by introducing a Lagrange multiplier λ_j for each constraint j and minimizing:

$$S(w, \lambda) = \sum_{ij} \Delta w_{ij}^2 + \sum_j \lambda_j \sum_i (\Delta w_{ij} x_i - w_{ij} \Delta x_i), \quad (3)$$

where $\Delta w_{ij} = w_{ij}^* - w_{ij}$. Optimizing Eq. 3 leads to the solution:

$$\Delta w_{ij} = -\lambda_j x_i / 2, \quad (4)$$

and the Lagrange multiplier can be determined by the constraints:

$$\lambda_j = -\frac{2 \sum_i w_{ij} \Delta x_i}{\sum_i x_i^2}, \quad (5)$$

which finally leads to an exact expression of the minimal duality weights as a linear function of the original weights:

$$w_{ij}^* = w_{ij} + \Delta w_{ij} = w_{ij} + \sum_{i'=1}^{L_1} b_{i'i} w_{i'j}, \quad (6)$$

where the linear coefficients $b_{i'i} = \frac{\Delta x_{i'} x_i}{\|\mathbf{x}\|^2}$ are determined entirely by properties of the input (sample), i.e., the correlation of the input (\mathbf{x}) and the difference ($\Delta \mathbf{x} \equiv \mathbf{x}' - \mathbf{x}$) between testing and training inputs (see Fig. 1B for an illustration).

The duality relation (Eq. 6) maps the ensemble of test inputs ($\{\mathbf{x}'\}$) in activity space (note that the original data is the activity of the input layer) to a corresponding distribution of dual weights ($\{\mathbf{w}^*\}$) in the weight space, which allows us to determine the generalization gap based on the dependence of the loss function on the weights, i.e., the loss landscape.

3 The generalization loss depends on both the loss landscape sharpness and the weight norm

For a given solution (weight vector) \mathbf{w} learnt from a set of training samples, the generalization performance can be characterized by the average loss of testing samples. Here, we define an individual generalization gap for a given test sample- k as

the difference between the loss of the test sample \mathbf{x}'_k and that of the closest training sample \mathbf{x}_k with the same label: $\Delta l_k \equiv l(\mathbf{w}, \mathbf{x}'_k) - l(\mathbf{w}, \mathbf{x}_k)$. For simplicity, we define closeness by using the Euclidean distance in this paper.

By using the A-W duality relation, we can rewrite the individual generalization gap as the difference in loss for the same input \mathbf{x}_k but with two sets of weights: the solution \mathbf{w} and the dual weights $\mathbf{w}_k^* = \mathbf{w} + \Delta \mathbf{w}_k$, which is shifted from the solution by $\Delta \mathbf{w}_k$. Note that the dual weights \mathbf{w}_k^* is sample dependent. For sample- k , \mathbf{w}_k^* can be obtained from Eq. 6 where the linear coefficient $b_{ii',k} = \frac{\Delta x_{i',k} x_{i,k}}{\|\mathbf{x}_k\|^2}$ for sample- k is determined by the inputs from the training and test sample pair: \mathbf{x}_k and $\mathbf{x}'_k = \mathbf{x}_k + \Delta \mathbf{x}_k$. From the weight shift vector $\Delta \mathbf{w}_k$, an “effective gradient” \mathbf{g}_k (vector) can be defined as:

$$\mathbf{g}_k \equiv \frac{\Delta l_k}{\|\Delta \mathbf{w}_k\|^2} \Delta \mathbf{w}_k. \quad (7)$$

By using \mathbf{g}_k , we can write the generalization gap for sample- k as:

$$\Delta l_k \equiv l(\mathbf{w}, \mathbf{x}'_k) - l(\mathbf{w}, \mathbf{x}_k) = l(\mathbf{w}_k^*, \mathbf{x}_k) - l(\mathbf{w}, \mathbf{x}_k) = \mathbf{g}_k \cdot \Delta \mathbf{w}_k. \quad (8)$$

Next, we express the two vectors \mathbf{g}_k and $\Delta \mathbf{w}_k$ in an orthogonal basis $\{\mathbf{e}_n\}$ with \mathbf{e}_n the unit vector in direction $n (= 1, 2, \dots, M)$: $\mathbf{g}_k = \sum_{n=1}^M g_{n,k} \mathbf{e}_n$ and $\Delta \mathbf{w}_k = \sum_{n=1}^M \Delta w_{n,k} \mathbf{e}_n$ with the components given by $g_{n,k} = \mathbf{g}_k \cdot \mathbf{e}_n$ and $\Delta w_{n,k} = \Delta \mathbf{w}_k \cdot \mathbf{e}_n$. Here, we can use the eigen-directions of the Hessian matrix ($\mathcal{H} = \nabla \nabla L|_{\mathbf{w}}$) of the overall training loss function (L) evaluated at the solution \mathbf{w} (another choice is the Fisher information matrix) as the basis. The overall generalization gap averaged over all testing samples is then:

$$\Delta L = \langle \Delta l_k \rangle_k = \sum_{n=1}^M \langle g_{n,k} \Delta w_{n,k} \rangle_k = \sum_{n=1}^M [c_n \sigma_{g,n} \sigma_{w,n} + \mu_{g,n} \mu_{w,n}], \quad (9)$$

where $\mu_{g,n} \equiv \langle g_{n,k} \rangle_k$ and $\mu_{w,n} \equiv \langle \Delta w_{n,k} \rangle_k$ are the average components; $\sigma_{g,n}^2 \equiv \langle g_{n,k}^2 \rangle_k - \mu_{g,n}^2$ and $\sigma_{w,n}^2 \equiv \langle \Delta w_{n,k}^2 \rangle_k - \mu_{w,n}^2$ are the corresponding variances; and c_n is the correlation coefficient between $g_{n,k}$ and $\Delta w_{n,k}$:

$$c_n \equiv \frac{\langle (g_{n,k} - \mu_{g,n})(\Delta w_{n,k} - \mu_{w,n}) \rangle_k}{\sigma_{g,n} \sigma_{w,n}}. \quad (10)$$

Given that the training and testing samples are from the same distribution, there is no correlation between \mathbf{x}_k and $\Delta \mathbf{x}_k$. Therefore, the sample averaged linear coefficient $\langle b_{i',k} \rangle_k = \langle \frac{\Delta x_{i',k} x_{i,k}}{\|\mathbf{x}_k\|^2} \rangle \approx 0$ and thus $|\mu_{w,n}| \ll \sigma_{w,n}$ and $|\mu_{g,n}| \ll \sigma_{g,n}$, which were verified

in our numerical experiments (see Fig. S1 in Supplementary Material (SM)). Thus, the $\mu_{g,n}\mu_{w,n}$ term in Eq. 9 is negligible, and the overall generalization gap can be decomposed into contributions (ΔL_n) from different directions in the weight-space:

$$\Delta L \approx \sum_{n=1}^M \Delta L_n = \sum_{n=1}^M c_n \sigma_{w,n} \sigma_{g,n}, \quad (11)$$

where each contribution $\Delta L_n = c_n \sigma_{w,n} \sigma_{g,n}$ is proportional to the standard deviation of gradients ($\sigma_{g,n}$) and the standard deviation of the dual weights ($\sigma_{w,n}$) among individual samples with a positive definite coefficient $0 \leq c_n \leq 1$, which does not show strong dependence on n (see Fig. S2 in SM). Note that the expression for the generalization gap given in Eq. 11 is exact and ΔL is highly correlated with the test error ϵ_{te} , both of which are verified empirically as shown in Fig. S3 in the SM. Next, we explain the geometrical meaning (interpretation) of the two determining factors (determinants) - $\sigma_{g,n}$ and $\sigma_{w,n}$ - that control generalization.

First, by ignoring the higher order correlations and taking the linear approximation (see SM for details), we can show that the gradient variance $\sigma_{g,n}^2 \approx \langle (g_{n,k}^{(0)})^2 \rangle_k$, where $g_{n,k}^{(0)} = \frac{\partial l_k}{\partial w_n}|_w$ is the gradient of the loss function l_k for sample- k in direction- n . Clearly, $\langle (g_{n,k}^{(0)})^2 \rangle_k$ is just the diagonal element of the expected (empirical) Fisher information matrix $\mathcal{F} \equiv \langle \nabla l_k \nabla l_k \rangle_k$. Since \mathcal{F} is equal to the Hessian matrix (\mathcal{H}) at the solution [11,12] up to a normalization constant, we have $\langle (g_{n,k}^{(0)})^2 \rangle_k \propto H_n$ with H_n the n -th eigenvalue of \mathcal{H} . To verify the connection between $\sigma_{g,n}^2$ and H_n without any approximation, we have computed the gradient variance $\sigma_{g,n}^2$ numerically for all the cases studied in this paper. As shown in Fig. 2A, $\sigma_{g,n}^2$ and H_n are highly correlated with a linear dependence at large values of $\sigma_{g,n}^2$ where $\sigma_{g,n}^2 \approx \langle (g_{n,k}^{(0)})^2 \rangle_k$ holds; the deviation from linearity at small $\sigma_{g,n}^2$ could be due to corrections from higher order correlations and other nonlinear effects. In our previous work [13], we defined a flatness F_n of loss landscape in direction- n based on a threshold for the loss function. As shown in Fig. S4 in SM, $\sigma_{g,n}$ is inversely correlated with F_n . Therefore, the first generalization determinant $\sigma_{g,n}$ measures the sharpness of the loss landscape in direction- n .

Second, the dual weight variance $\sigma_{w,n}^2$ measures the variation of the dual weight change vector $\Delta \mathbf{w}_k$ projected onto direction- n among all samples. From the expression of the minimal dual weights in Eq. 6, we have:

$$\|\sigma_w\|^2 \equiv \sum_{n=1}^M \sigma_{w,n}^2 = \sum_{i=1}^{L_1} \sum_{i'=1}^{L_1} \sum_{j=1}^{L_2} C_{ii'} w_{ij} w_{i'j}, \quad (12)$$

where $C_{ii'} = \langle \frac{\Delta x_{i,k} \Delta x_{i',k}}{\|x_k\|^2} \rangle_k$ is the covariance matrix of the relative difference $\Delta \mathbf{x} / \|\mathbf{x}\|_2$ of the input \mathbf{x} between training and testing samples. Note that $C_{ii'}$ depends only on the input activity and is independent of the weight \mathbf{w} itself. From the quadratic form of Eq. 12, it is clear that $\|\sigma_{\mathbf{w}}\|$ represents a distance measure of the solution \mathbf{w} weighted by the data-dependent covariance matrix C . Indeed, as shown in Fig. 2B, $\|\sigma_{\mathbf{w}}\|^2$ scales with the L_2 -norm of the solution $\|\mathbf{w}\|_2$ in all the cases studied in this paper. Thus, the second generalization determinant $\sigma_{w,n}$ represents a data-weighted distance of the solution to the origin ($\mathbf{w} = \mathbf{0}$) along direction- n , which characterizes the size of the solution for a given data set.

The dependence of generalization on the two geometrical determinants as revealed in Eq. 11 indicates two general ways to improve generalization: by finding flatter solutions and/or by finding solutions with a smaller weight norm. In the following section, we show how some of the well-known algorithms and techniques for improving generalization follow exactly these strategies or combination of both.

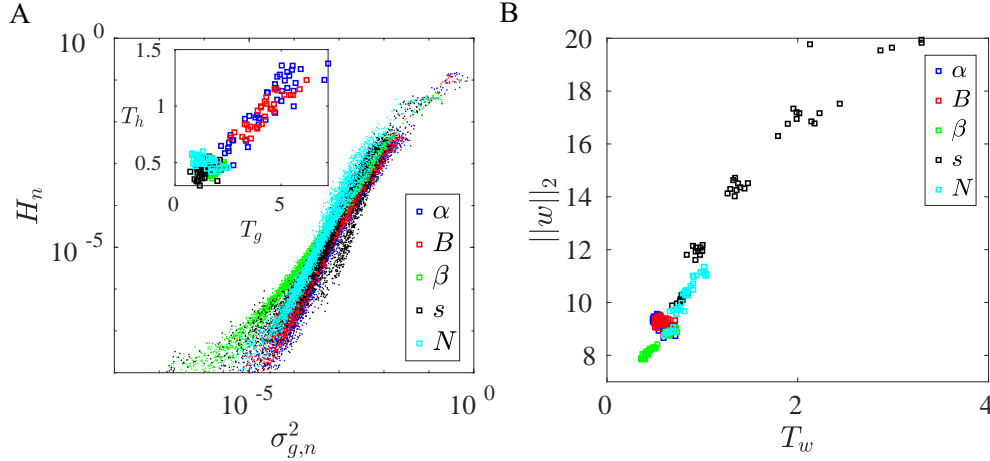


Figure 2: (A) Hessian eigenvalue H_n versus $\sigma_{g,n}^2$ for all hyperparameters (learning rate α and batch size B in SGD; decay rate β and initial weight scale s) and sample size (N) studied in this paper. The inset shows the trace of the Hessian ($T_h \equiv \sum_{i=1}^N H_i$) is highly correlated with the total gradient variance $T_g \equiv \sum_{i=1}^N \sigma_{g,i}^2$. (B) L_2 -norm of the weight $\|\mathbf{w}\|_2$ versus the total dual weight variance $T_w \equiv \sum_{n=1}^N \sigma_{w,n}^2$. Both L_2 norm and S_w remain roughly constant when α and B are varied. When β and s are varied, $\|\mathbf{w}\|_2$ changes significantly, and T_w increases with $\|\mathbf{w}\|_2$.

4 Understanding generalization through the lens of the two geometric determinants

Given the two geometric determinants for generalization, we can evaluate and understand the effects of various (implicit and explicit) regularization schemes in neural network based learning and their abilities for finding more generalizable solutions.

We first train neural network models to reach different solutions by tuning hyperparameters (batch size and learning rate) in stochastic gradient descent (SGD), or by using explicit regularization schemes such as weight decay with different decay rates. We then study the generalization gap of the solution, and its dependence on the hyperparameters (batch size/learning rate in SGD and decay rate in weight decay) through the lens of the two geometric determinants found through the A-W duality. Specifically, at each solution, we computed the values of the two standard deviations ($\sigma_{g,n}$ and $\sigma_{w,n}$) in each eigen-direction n , and the correlation constant c_n . The generalization gap is decomposed into the contributions from different eigen-directions according to Eq. 11. Consistent with previous studies [13, 14], we found that there are only a small number of sharp directions characterized by large values of $\sigma_{g,n}$, and the loss landscape in the majority of the eigen-directions is flat with much smaller values of $\sigma_{g,n}$. However, these few sharp directions contribute to a significant fraction of the total generalization loss, e.g., in the example shown in Fig. 3, more than 50% of the generalization loss comes from the 10 sharpest directions in the 900 dimensional weight space. To quantify the contributions from the sharp directions and the rest of the (flat) directions, we separate the generalization loss into two parts: $\Delta L = \Delta L_s + \Delta L_f$ with $\Delta L_s = \sum_{n=1}^{n_s} \Delta L_n$ and $\Delta L_f = \sum_{n=n_s+1}^N \Delta L_n$ corresponding to the generalization loss from the sharp and flat directions, respectively, where n is the rank order according to $\sigma_{g,n}$ and n_s is the number of the sharp directions, which is determined by the value of n with the steepest decrease in $\sigma_{g,n}$ (the cumulative variance of the few sharp directions reaches $\sim 50\%$ of the total variance).

In previously proposed sharpness-based measures [8, 9] for generalization, only the sharpest direction(s) is considered. As we show below, one of the main insights gained from our study is that both ΔL_s and ΔL_f contribute significantly but differently to the overall generalization gap. As a result, they can be regularized and controlled independently or together to improve generalization.

4.1 Finding flatter solutions by tuning SGD hyperparameters

We first change the learning rate α in SGD (with a fixed batch size) to obtain different solutions. We then analyze the solutions in terms of the generalization gap and its dependence on loss function sharpness (σ_g) and solution size (σ_w), see Methods for details. In Fig. 3A, we plotted the “sharpness” spectrum, i.e., $\sigma_{g,n}$ versus n for different values of α , which clearly shows that as α increases, the values of $\sigma_{g,n}$ in the sharpest directions ($n \leq n_s$) are reduced while they do not change significantly in the flatter directions ($n > n_s$). However, as shown in Fig. 3B, changing α does not significantly affect $\sigma_{w,n}$ across all the directions (Note that we plotted the accumulative sum $S_{w,n} \equiv \sum_{i=1}^n \sigma_{w,i}$ to smooth out the noise in $\sigma_{w,n}$). As a result, the generalization gap ΔL decreases when the learning rate increases from 0.005 to 0.1 (further increase of α leads to non-convergence). More importantly, we find that the improvement in generalization for larger α is mainly due to the reduction of ΔL_s in the sharp directions while the contribution from the flat directions ΔL_f remains unchanged, which can be explained by the dependence of the two generalization determinants on α shown in Fig. 3A&C.

We next changed batch size B (with a fixed α) to obtain different solutions. By carrying out the same analysis as for changing α , we found that increasing B has the opposite effects as increasing α . As shown in Fig. 3D-F, a larger B leads to solutions where the sharpness parameters $\sigma_{g,n}$ in the sharpest directions increases, which leads to a larger generalization gap that originates from the increase in the contribution ΔL_s from the sharpest directions.

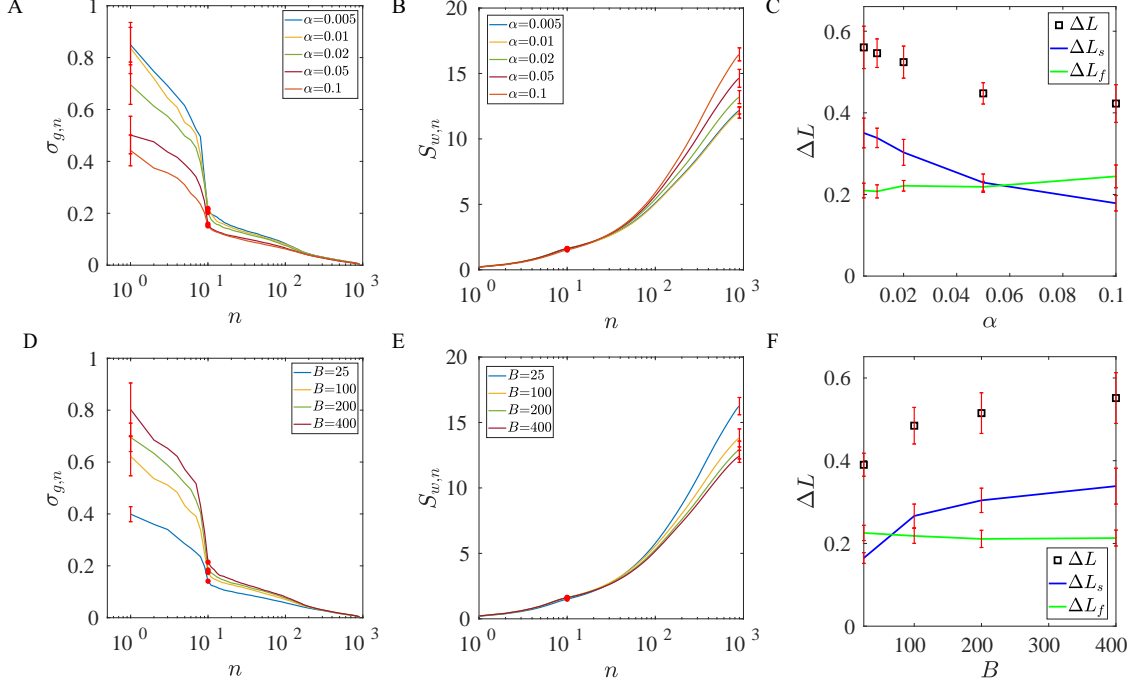


Figure 3: The effects of the learning rate α or the batch size B in SGD on generalization. (A) The sharpness spectrum $\sigma_{g,n}$ versus n for different learning rates. (B) The accumulative size $S_{w,n} = \sum_{i=1}^n \sigma_{w,i}$ for different learning rates. (C) The generalization gap (ΔL) and the contributions from the sharp and flat directions (ΔL_s and ΔL_f) versus α . (D-F) The same as (A-C) but for varying batch size B . All components are ordered by the decreasing order of $\sigma_{g,n}$ (from sharp directions to flat directions). As shown in (A) and (D), when increasing α or decreasing B , the sharpness ($\sigma_{g,n}$) decreases in the dominant components ($n \leq n_s$) while $S_{w,n}$ does not change significantly as shown in (B)&(E). As a result, the decrease in generalization loss comes mainly from the contribution from the sharp directions ΔL_s (blue lines) as shown in (C)&(F). Each line is averaged over 10 independent realization and the error bar represents the standard deviation. $n_s = 10$ (red dots) in this study. $B = 25$ in (A-C) and $\alpha = 0.1$ in (D-F).

4.2 Smaller solutions are more generalizable: effects of weight decay and initialization

Another important regularization scheme to enhance generalization is by introducing weight decay in the learning dynamics. The weight decay scheme is equivalent to adding a regularization term that is proportional to the L_2 norm of the weight vector, $\beta||\mathbf{w}||^2$, where the coefficient β is a hyperparameter corresponding to the decay rate of weights. As shown in Fig. 4A&B, the sharpness of the solution does not depend on β while the size of the solution characterized by the accumulative sum $S_{w,n} \equiv \sum_{i=1}^n \sigma_{w,i}$ is smaller when β increases. As a result, the generalization gap ΔL decreases as the decay rate β increases from 0 to 0.02, similar to the case when the learning rate α is increased. However, in contrast to the case of increasing learning rate α , ΔL_s does not change significantly with β and the reduction of ΔL comes mostly from the decrease of ΔL_f with increasing β , as shown in Fig. 4C. The reduction in $\sigma_{w,n}$ is stronger in the flat directions since the resistance to weight reduction (decay) is weaker in flatter directions (see Fig. S5 in SM), which explains the significant reduction in ΔL_f but not in ΔL_s . Thus, our analysis shows that the enhancement of generalization by using weight decay is achieved predominantly by reducing the size of the solution, i.e., the second determinant of generalization.

To further elucidate the effect of solution size on generalization, we look for solutions of different sizes by using different initializations. In our experiment, the weights are initialized by Xavier initialization where weights are drawn randomly from a uniform distribution with a hyperparameter s that determines the range of the uniform distribution. As shown in Fig. 4D-F, the increase of s has the opposite effects as compared with increasing β . As s increases, the network finds solutions with similar sharpness spectra $\sigma_{g,n}$ but an increasing size as measured by $S_{w,n}$ shown in Fig. 4. This leads to an increase in the generalization gap ΔL , which comes mostly from the increase of the contribution from the flat directions ΔL_f . These results confirm that a smaller solution with the same sharpness has a higher generalizability as shown by our theory.

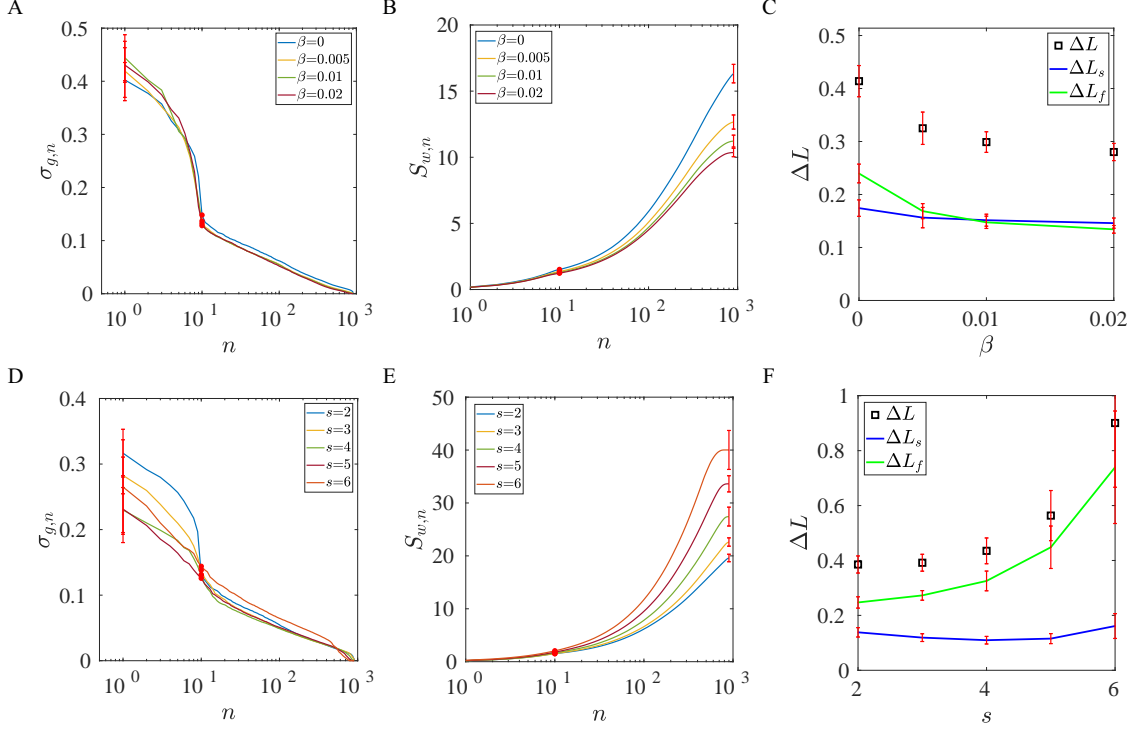


Figure 4: The effects of the weight decay rate β or the weight initiation s in SGD on generalization. (A) The sharpness spectrum $\sigma_{g,n}$ versus n for different values of β . (B) The accumulative size sum $S_{w,n} = \sum_{i=1}^n \sigma_{w,i}$ for different values of β . (C) The generalization gap (ΔL) and the contributions from the sharp and flat directions (ΔL_s and ΔL_f) versus β . (D-F) The same as (A-C) but for different values of s . All components are ordered by the decreasing order of $\sigma_{g,n}$ (from sharp directions to flat directions). As shown in (A) and (D), when increasing β or decreasing s , the sharpness ($\sigma_{g,n}$) does not change significantly while $S_{w,n}$ decreases as shown in (B)&(E). As a result, the decrease in generalization loss comes mainly from the reduction of the loss from the flat directions ΔL_f (green lines) as shown in (C)&(F). $B = 25$ and $\alpha = 0.1$ are used.

4.3 The effects of dropout, data size, and mislabeled data

So far, we used SGD and weight decay as two representative examples to highlight the dependence of the generalization gap on either one of the two determinants, the sharpness of the loss landscape at the solution and the size of the solution, respectively. In general, both determinants can be affected, albeit in different ways depending on the regularization scheme used and specifics of the data set. For example, another popular regularization scheme is dropout [15] where a randomly selected subset of neurons (and their connected weights) are dropped during each iteration. We find that both the sharpness of loss landscape and the size of the solution are affected by the dropout fraction d but in opposite ways. As d increases from zero, $\sigma_{g,n}$ in the sharpest directions first decrease significantly before saturating to fixed values while $\sigma_{w,n}$ continuously increase with d (see Fig. S6A&B in SM). At low d , ΔL is dominated by ΔL_s , which decreases with d . At high d , ΔL is dominated by ΔL_f , which increases with d . As a result, the generalization gap has a non-monotonic dependence on d as shown in Fig. S6C in SM.

In addition to various regularization schemes, we have studied the effects of the size (N) of the training data set. We found that both $\sigma_{g,n}$ and $\sigma_{w,n}$ change with N : the solution becomes flatter across all directions but also slightly larger as shown in Fig. S7A-D in the SM. In addition, the correlation coefficient c_n decreases with N (see Fig. S7C in the SM), which also contributes to reducing the generalization gap in all directions. The combined effect is that even though the reduction in ΔL comes largely from the reduction of ΔL_s from the sharp direction the decrease of ΔL_f with N is not negligible, i.e., increasing N improves generalization in all directions across the sharpness spectrum.

We have also investigated the case where a fraction (ρ) of the training data have random labels (see Fig. S7E-H in SM) [7, 16]. As expected, the generalization gap (ΔL) increases with ρ (Fig. S7H in SM). As ρ increases, the sharpness of all the flat directions ($n > n_s$) increases significant while the sharpness of the few sharpest directions ($n \leq n_s$) decreases (Fig. S7E). For a finite ρ , the sharpness spectrum is continuous without a sudden drop seen in the case with $\rho = 0$ – the network needs to use all weight directions to memorize the random labels of the mislabeled data. Besides sharpness, the size of the solution also increases with ρ . In addition, the correlation coefficient c_n increases with ρ for all n . The combined effect is that ΔL is dominated by ΔL_f , which increases with ρ due to the increase of both the sharpness $\sigma_{g,n}$ and the size $\sigma_{w,n}$ in almost all the directions ($n > n_s$).

5 Discussion

In this work, we prove a duality between the changes in the activities of the neurons in a given layer of neurons and the changes of the weights originating from this layer to the next. By using the duality relation, we showed that the generalization loss can be decomposed into contributions from different eigen-directions in the weight space and the contribution from each direction depends on the sharpness of the loss landscape as well as the size of the solution along that direction, which are the two geometric determinants for generalization.

The notion that flat minima correspond to more generalizable solutions was first put forth by Hochreiter and Schmidhuber in 1997 [17]. Empirical evidence in DLNN were found in support of this idea [9, 18], which has been used to develop algorithms searching for flatter minima [19–21] to improve generalization. However, as first pointed out by Dinh et al [10], the loss function of a feed forward network is invariant under a simple scaling transformation in which the weights in one layer are multiplied by a common scaling factor p and the weights in the next layer is scaled by p^{-1} . This scale invariance means that one can always find a solution whose sharpness in a given layer is arbitrarily large without affecting its generalization loss. Flatness has the dimension of weight, which is different from that of the loss function. Therefore, even on a purely dimensional ground, flatness can not be the only determinant for generalization. The key question is that when we say the loss landscape is flat, what is it compared with? Here, we show that the flatness of the loss landscape in a given direction should be compared with the variation of the dual weights σ_w in that direction to determine its effect on generalization. This second determinant is related to the weight norm, which is another popular measure of generalization [22–25]. However, weight norm alone has not been a successful measure of generalization in DLNN [8]. One of the main insights gained from our study is that these two determinants together determine generalization. For the scale transformation proposed by Dinh et al [10], the sharpness (σ_g) in a given layer scales by p , and the weight variation (σ_w) in the same layer scales by p^{-1} , which makes the expression for generalization gap (Eq. 11) scale invariant as it should be.

The A-W duality and the resulting decomposition of the generalization gap are valid in any densely connected layer such as fully connected layers (FCL). We have used these results in different intermediate FCLs in a multilayer fully connected network (FCN) to test the effects of different regularization schemes on generalization. As shown in Fig. S8 and Fig. S9 in the SM, the loss landscape becomes flatter and the solution becomes larger as the layer becomes closer to the output layer with the overall dependence of the generalization gap on the two geometric determinants

and different hyperparameters remaining the same as reported in the main text for a given FCL (Figs. 3&4). How these two determinants evolve through the network (from the input layer to the output layer) and how these evolutions relate to previous work based on the information bottleneck idea [26, 27] remain interesting open questions. We have also carried out our analysis to FCLs in a Convolution Neural Network (CNN) and the results are consistent with those from a FCN (see Fig. S10 in SM). For a convolutional layer, there is no exact duality relation due to the relatively small number of weights for each filter. However, the general idea of looking for equivalence between activity and weight changes may be worth pursuing. For example, one may obtain an approximate duality relation, e.g., by minimizing the difference of the outputs $||\phi(\mathbf{x}, \mathbf{w}) - \phi(\mathbf{x}', \mathbf{w}')||$. If such an approximate duality relation leads to a good approximation of the overall loss function, we expect the general conclusions reached here for a FCL would still be valid.

Our results provide a unified framework to understand how various regularization schemes (implicit and explicit) improve generalization. For SGD, generalization improves as the learning rate α increases (or batch size B decreases) within a certain range. We found that the improvement in generalization originates predominantly from the reduction of the sharpness of the loss function along the few sharpest directions. Previous work [11, 13, 28] showed that there is an anisotropic landscape dependent noise in SGD, which drives the system away from sharp minima. Since the strength of the SGD noise scales with α/B , the preference for flat minima is stronger for larger α and smaller B , which explains the improved generalization as α increases (or B decreases) shown in Fig. 3. In fact, the dependence of generalization on the two SGD hyperparameters (α and B) collapsed onto a single dependence of ΔL on α/B as shown in Fig. S11 in the SM. The improvement in generalization with weight norm regularization (weight decay) follows a different strategy that predominantly controls the second determinant, i.e., the size of the solution. The reduction in weight is more pronounced in the flatter directions in which the resistance for weight change is weaker. As a result, the reduction of the generalization comes from the majority flat directions. Going forward, the insights gained from our analysis of the key determinants for generalization may provide general guidance in developing new algorithms and/or regularization schemes to improve generalization.

6 Methods

Data Set and Neural Network Architecture. We used a subset of MNIST dataset or CIFAR-10 dataset as our training data. The subset contains all ten

classes, with N training images per class. The size of test data is 1,000 images for both case.

For MNIST experiment, we trained two fully connected networks with multiple hidden layers where l th hidden layer contains H_l hidden units. In the main text, we did the experiments on a network with two hidden layers, and each hidden layer contains 30 hidden units ($L_1 = L_2 = 30$). In the SM, we showed the experimental results of a network with four hidden layers, where each layer has the same number of hidden units ($L_1 = L_2 = L_3 = L_4 = 30$).

For the CIFAR-10 dataset, we used a convolutional neural network with two convolutional layers and four fully connected layers. The size of two convolutional layers are $3 \times 5 \times 5 \times 6$ and $6 \times 5 \times 5 \times 16$, where the size is denoted by number of input channels \times kernel size \times kernel size \times number of output channels. Each convolutional layer is followed by a max-pooling layer with size 2×2 . The size of four fully connected layers are 400, 120, 25, 10.

Simulation Details. Unless stated otherwise, the default hyperparameters and data size are: $\alpha = 0.1, B = 25, \beta = 0, s = 1, N = 400, \rho = 0, d = 0$. Stochastic gradient descent (SGD) was used for training.

The weights are initialized by Xavier initialization: weights are drawn from a uniform distribution $U(-\frac{s\sqrt{6}}{\sqrt{n_i+n_{i+1}}}, \frac{s\sqrt{6}}{\sqrt{n_i+n_{i+1}}})$, where n_i is the number of incoming connections to the layer and n_{i+1} is the number of ongoing connections from the layer.

During training, a weight-decay regularization with decay rate β is used for the first 200 epochs. The weights are considered to be a solution when its corresponding training error reaches 0. In practical, we stop the training when training loss first reached a low threshold $= 5 \times 10^{-4}$ for MNIST experiments and 1×10^{-3} for CIFAR-10 experiments.

Analysis Details. Once the network is trained to the predefined accuracy, we analyze the solution in the following way:

1. For each test data, we calculate its Euclidean distance with all training data and find its closest partner.
2. Choose two layers with full connection and calculate the dual weight for each test data by using the activity-weight duality relation. For each pair of training data and test data, we first calculate the neural activities x_i for the chosen layer and obtain the neural activity difference Δx_i between training data and test data. With x_i and Δx_i , the minimal duality solution is obtained by applying Eq. 6. In MNIST experiments, we did the activity-weight duality analysis

between two hidden layers; In CIAFR-10 experiments, we did the analysis between two fully connected hidden layers with size 120×25 .

3. The dual weight w^* and the effective gradient g were determined from Eqs. 6&7, respectively. The two vectors are projected onto the eigen-directions of Hessian matrix. The standard deviations of the n -th components, $\sigma_{g,n}$ and $\sigma_{w,n}$, as well as the correlation coefficient c_n between them were computed. The generalization gap was computed by using Eq. 11.

7 Acknowledgments

We thank Ken Clarkson and Roger Traub for careful reading of our manuscript and useful comments. The work by FY was partially done while he was employed as an IBM intern.

References

- [1] LeCun, Y., Bengio, Y. & Hinton, G. Deep learning. *Nature* **521**, 436 EP – (2015). URL <https://doi.org/10.1038/nature14539>.
- [2] Goodfellow, I., Courville, A. & Bengio, Y. *Deep learning*, vol. 1 (MIT Press, 2016).
- [3] He, K., Zhang, X., Ren, S. & Sun, J. Deep residual learning for image recognition. In *Proceedings of the IEEE conference on computer vision and pattern recognition*, 770–778 (2016).
- [4] Wu, Y. *et al.* Google’s neural machine translation system: Bridging the gap between human and machine translation. *arXiv preprint arXiv:1609.08144* (2016).
- [5] Silver, D. *et al.* Mastering the game of go with deep neural networks and tree search. *Nature* **529**, 484–489 (2016). URL <https://doi.org/10.1038/nature16961>.
- [6] Callaway, E. ‘it will change everything’: Deepmind’s ai makes gigantic leap in solving protein structures. *Nature* **588**, 203–204 (2020). URL <https://doi.org/10.1038/d41586-020-03348-4>.

- [7] Zhang, C., Bengio, S., Hardt, M., Recht, B. & Vinyals, O. Understanding deep learning requires rethinking generalization (2016). 1611.03530.
- [8] Jiang, Y., Neyshabur, B., Mobahi, H., Krishnan, D. & Bengio, S. Fantastic generalization measures and where to find them. *ICLR* (2020).
- [9] Keskar, N. S., Mudigere, D., Nocedal, J., Smelyanskiy, M. & Tang, P. T. P. On large-batch training for deep learning: Generalization gap and sharp minima. *ArXiv* **abs/1609.04836** (2016).
- [10] Dinh, L., Pascanu, R., Bengio, S. & Bengio, Y. Sharp minima can generalize for deep nets (2017). 1703.04933.
- [11] Zhu, Z., Wu, J., Yu, B., Wu, L. & Ma, J. The anisotropic noise in stochastic gradient descent: Its behavior of escaping from sharp minima and regularization effects. In *Proc. Int. Conf. Mach. Learn.*, 7654–7663 (2019).
- [12] Martens, J. New insights and perspectives on the natural gradient method. *arXiv preprint arXiv:1412.1193* (2014).
- [13] Feng, Y. & Tu, Y. The inverse variance–flatness relation in stochastic gradient descent is critical for finding flat minima. *Proceedings of the National Academy of Sciences* **118** (2021).
- [14] Sagun, L., Evci, U., Guney, V. U., Dauphin, Y. & Bottou, L. Empirical analysis of the hessian of over-parametrized neural networks (2017). 1706.04454.
- [15] Srivastava, N., Hinton, G. E., Krizhevsky, A., Sutskever, I. & Salakhutdinov, R. Dropout: a simple way to prevent neural networks from overfitting. *J. Mach. Learn. Res.* **15**, 1929–1958 (2014).
- [16] Feng, Y. & Tu, Y. Phases of learning dynamics in artificial neural networks in the absence or presence of mislabeled data. *Machine Learning: Science and Technology* **2**, 043001 (2021).
- [17] Hochreiter, S. & Schmidhuber, J. Flat minima. *Neural Computation* **9**, 1–42 (1997).
- [18] Wei, C. & Ma, T. Improved sample complexities for deep networks and robust classification via an all-layer margin (2021). 1910.04284.

- [19] Chaudhari, P. *et al.* Entropy-sgd: Biasing gradient descent into wide valleys (2016). 1611.01838.
- [20] Foret, P., Kleiner, A., Mobahi, H. & Neyshabur, B. Sharpness-aware minimization for efficiently improving generalization (2021). 2010.01412.
- [21] Baldassi, C., Pittorino, F. & Zecchina, R. Shaping the learning landscape in neural networks around wide flat minima. *Proceedings of the National Academy of Sciences* **117**, 161–170 (2020). URL <https://www.pnas.org/content/117/1/161>. <https://www.pnas.org/content/117/1/161.full.pdf>.
- [22] Neyshabur, B., Tomioka, R. & Srebro, N. Norm-based capacity control in neural networks (2015). 1503.00036.
- [23] Bartlett, P., Foster, D. J. & Telgarsky, M. Spectrally-normalized margin bounds for neural networks (2017). 1706.08498.
- [24] Neyshabur, B., Li, Z., Bhojanapalli, S., LeCun, Y. & Srebro, N. Towards understanding the role of over-parametrization in generalization of neural networks (2018). 1805.12076.
- [25] Nagarajan, V. & Kolter, J. Z. Generalization in deep networks: The role of distance from initialization (2019). 1901.01672.
- [26] Tishby, N. & Zaslavsky, N. Deep learning and the information bottleneck principle. *2015 IEEE Information Theory Workshop (ITW)* (2015). URL <http://dx.doi.org/10.1109/ITW.2015.7133169>.
- [27] Shwartz-Ziv, R. & Tishby, N. Opening the black box of deep neural networks via information. *arXiv preprint arXiv:1703.00810* (2017).
- [28] Chaudhari, P. & Soatto, S. Stochastic gradient descent performs variational inference, converges to limit cycles for deep networks. *2018 Information Theory and Applications Workshop (ITA)* (2018). URL <http://dx.doi.org/10.1109/ita.2018.8503224>.

Supplemental Material

Leading order approximation for $\sigma_{g,n}$

Following the procedure for defining partial derivatives in multi-dimensional space, we can write Δl_k as the sum of differences between the functional values at two coordinates that differ only along one of the basis directions:

$$\Delta l_k = \sum_{n=1}^N [l(\mathbf{w} + \Delta \tilde{\mathbf{w}}_{n,k}, \mathbf{x}_k) - l(\mathbf{w} + \Delta \tilde{\mathbf{w}}_{(n-1),k}, \mathbf{x}_k)], \quad (13)$$

where $\Delta \tilde{\mathbf{w}}_{n,k} = (\Delta w_{1,k}, \Delta w_{2,k}, \dots, \Delta w_{n,k}, 0, \dots, 0)$ is the projection of $\Delta \mathbf{w}_k$ onto the first n directions. Note that $\Delta \tilde{\mathbf{w}}_{n,k} - \Delta \tilde{\mathbf{w}}_{(n-1),k} = (\Delta \mathbf{w}_k \cdot \mathbf{e}_n) \mathbf{e}_n = \Delta w_{n,k} \mathbf{e}_n$ is the projection of $\Delta \mathbf{w}_k$ onto direction- n and we can define $d(n, k) \equiv l(\mathbf{w} + \Delta \tilde{\mathbf{w}}_{n,k}, \mathbf{x}_k) - l(\mathbf{w} + \Delta \tilde{\mathbf{w}}_{(n-1),k}, \mathbf{x}_k)$ as the change of loss along direction- n .

The overall generalization gap can be written as: $\Delta L = \sum_n \langle d(n, k) \rangle_k$. If we neglect the effect of correlation between different components of $\Delta \mathbf{w}$ on the loss function, we can approximate $\langle d(n, k) \rangle_k$ by taking all the unchanged weight components in $l(\mathbf{w} + \Delta \tilde{\mathbf{w}}_{n,k}, \mathbf{x}_k)$ and $l(\mathbf{w} + \Delta \tilde{\mathbf{w}}_{(n-1),k}, \mathbf{x}_k)$ to be their average values (over k):

$$\langle d(n, k) \rangle_k \approx \langle l(\mathbf{w} + \Delta w_{n,k} \mathbf{e}_n, \mathbf{x}_k) - l(\mathbf{w}, \mathbf{x}_k) \rangle_k, \quad (14)$$

where we have used the fact that $\langle \Delta \mathbf{w} \rangle_k = \mathbf{0}$.

By using linear approximation, the expression in Eq. 14 can be further simplified to: $\langle d(n, k) \rangle_k \approx g_{n,k}^{(0)} \Delta w_{n,k} =$ where $g_{n,k}^{(0)} = \frac{\partial l_k}{\partial w_n}|_{\mathbf{w}}$ is the gradient of the loss function l_k for sample- k in direction- n . Thus, the generalization can be expressed as:

$$\Delta L = \langle l(\mathbf{w} + \Delta \mathbf{w}_k, \mathbf{x}_k) - l(\mathbf{w}, \mathbf{x}_k) \rangle_k = \sum_{n=1}^N \langle g_{n,k} \Delta w_{n,k} \rangle_k \quad (15)$$

$$\approx \sum_{n=1}^N \langle l(\mathbf{w} + \Delta w_{n,k} \mathbf{e}_n, \mathbf{x}_k) - l(\mathbf{w}, \mathbf{x}_k) \rangle_k \quad (16)$$

$$\approx \sum_{n=1}^N \left\langle g_{n,k}^{(0)} \Delta w_{n,k} \right\rangle_k, \quad (17)$$

where the two successive approximations are made by ignoring higher order correlation effects and taking the linear approximation, respectively. Thus, the leading order approximation of $\sigma_{g,n}^2 \approx \left\langle (g_{n,k}^{(0)})^2 \right\rangle_k$, which is the diagonal elements of the Fisher information matrix $\mathcal{F} = \langle \nabla l_k \nabla l_k \rangle_k$ at the solution \mathbf{w} .

Supporting Figures

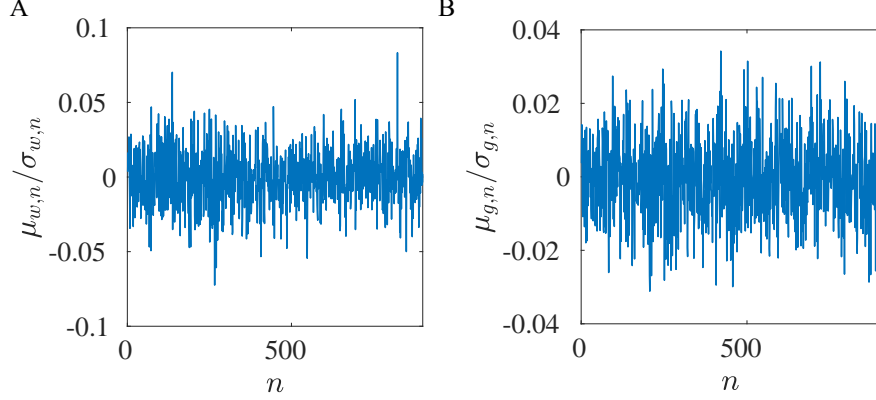


Fig. S1: The average components $\mu_{w,n}$ and $\mu_{g,n}$ relative to the corresponding standard deviations $\sigma_{w,n}$ and $\sigma_{g,n}$. From our results, it is clear that $|\mu_{w,n}| \ll \sigma_{w,n}$ and $|\mu_{g,n}| \ll \sigma_{g,n}$. Results are averaged over 10 independent realizations, hyperparameters used: $\alpha = 0.1$, $B = 25$.

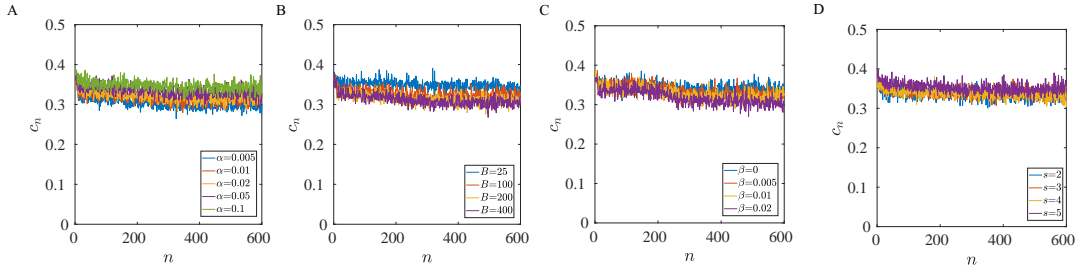


Fig. S2: The correlation coefficient c_n for different hyperparameters. c_n does not change significantly with n except for very large n where the contributions to the generalization loss is negligible. Except for adding new data (correctly labeled data or mislabeled data), c_n remain roughly constant independent of the hyperparameters.

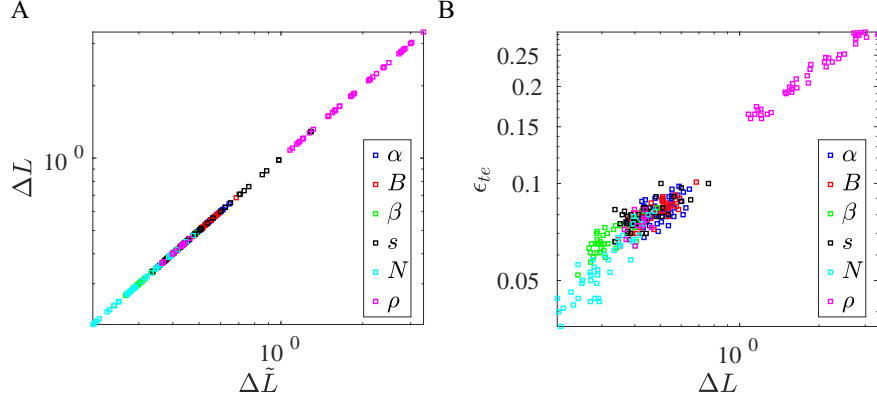


Fig. S3: (A) Generalization gap $\Delta \tilde{L} = L_{te} - L_{tr} = \langle l(\mathbf{x}_k, \mathbf{w}) - l(\mathbf{x}'_k, \mathbf{w}) \rangle_k$ computed directly from data versus ΔL determined from Eq. 11 using the A-W duality. (B) The test error ϵ_{te} versus ΔL (note the training error $\epsilon_{tr} = 0$ in the examples shown here).

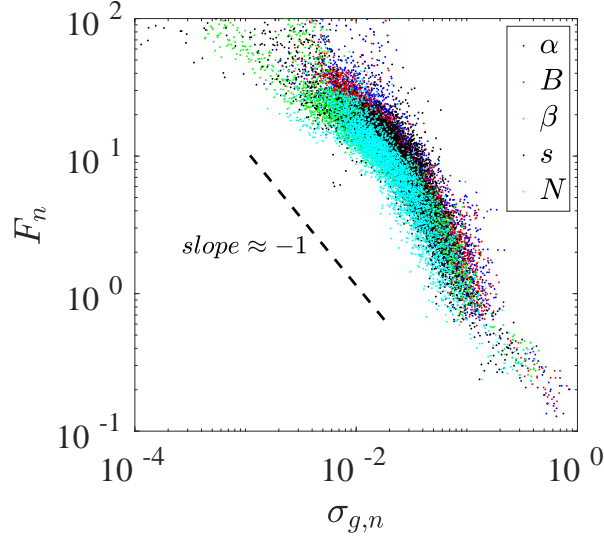


Fig. S4: Flatness F_n versus $\sigma_{g,n}^2$. Following [13], the flatness F_n in direction- n is defined as the width of the region along direction- n , within which the loss function changes within a factor of 2.

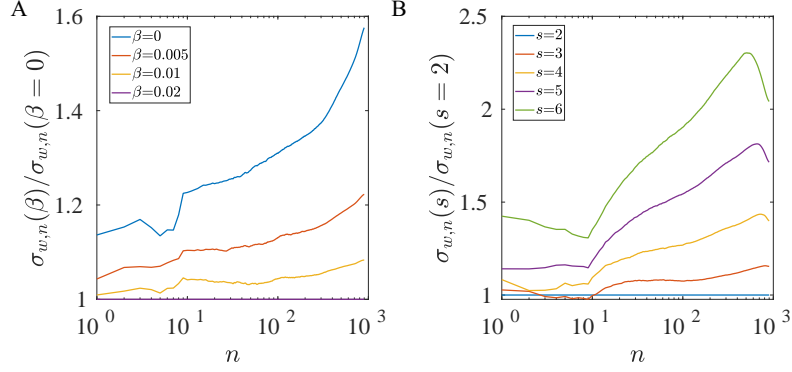


Fig. S5: The ratio of the weight variance for different weight decay rate and the weight initialization. (A) $\frac{\sigma_{w,n}(\beta)}{\sigma_{w,n}(\beta=0)}$; (B) $\frac{\sigma_{w,n}(s)}{\sigma_{w,n}(s=2)}$.

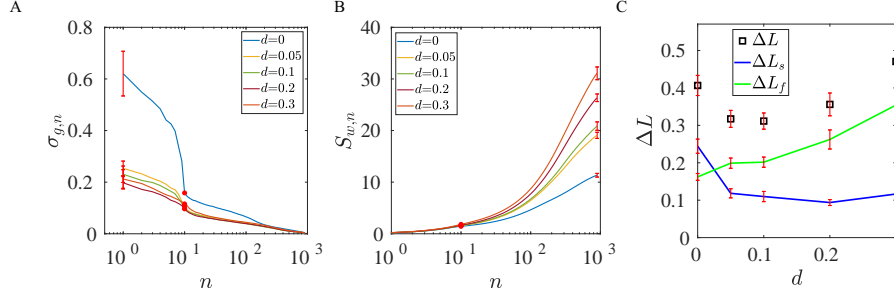


Fig. S6: The effects of changing dropout fraction d . (A) The sharpness spectrum $\sigma_{g,n}$. (B) The accumulative size $S_{w,n} = \sum_{i=1}^n \sigma_{w,i}$. (C) The generalization gap ΔL and the contributions from the sharp and flat directions, ΔL_s and ΔL_f , respectively. All components are ordered by the decreasing order of $\sigma_{g,n}$ (from sharp directions to flat directions).

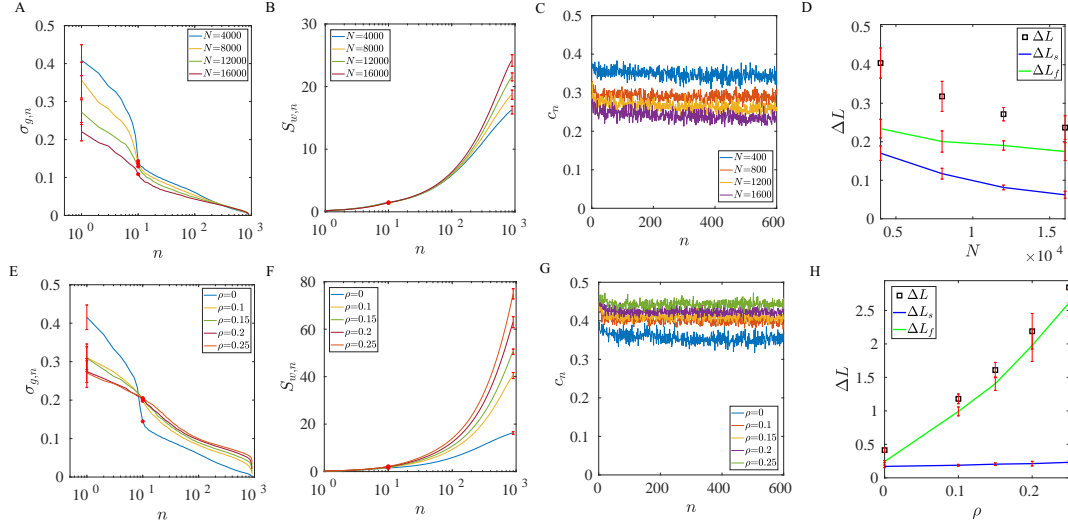


Fig. S7: The effects of the data set size N and the mislabeled fraction ρ . (A-D) and (E-H) show the sharpness spectrum $\sigma_{g,n}$, the accumulative size $S_{w,n} = \sum_{i=1}^n \sigma_{w,i}$, the correlation coefficient c_n , and the generalization gap (ΔL) together with the contributions from the sharp and flat directions (ΔL_s and ΔL_f), for different N and different ρ , correspondingly. All components are ordered by the decreasing order of $\sigma_{g,n}$ (from sharp directions to flat directions). (A) The sharpness ($\sigma_{g,n}$) decreases in all directions. (B) The accumulative size $S_{w,n}$ increases slightly. (C) The correlation coefficient c_n decreases with N . (D) The decrease in generalization loss (ΔL) comes from both the sharp directions (ΔL_s) and the flat directions (ΔL_f). (E) For a finite $\rho = 0.1, 0.15, 0.2, 0.25$, the sharpness ($\sigma_{g,n}$) increases significantly in the flat directions ($n > n_s$) while it decreases in the sharp directions, which makes the sharpness spectrum continuous (smooth) without a sudden jump as in the case with $\rho = 0$. (F) The size of the solution $S_{w,n}$ increases significantly with ρ . (G) The correlation coefficient c_n increases with ρ . (H) The increase in the overall generalization gap ΔL with ρ comes dominantly from the flat directions ΔL_f (green line).

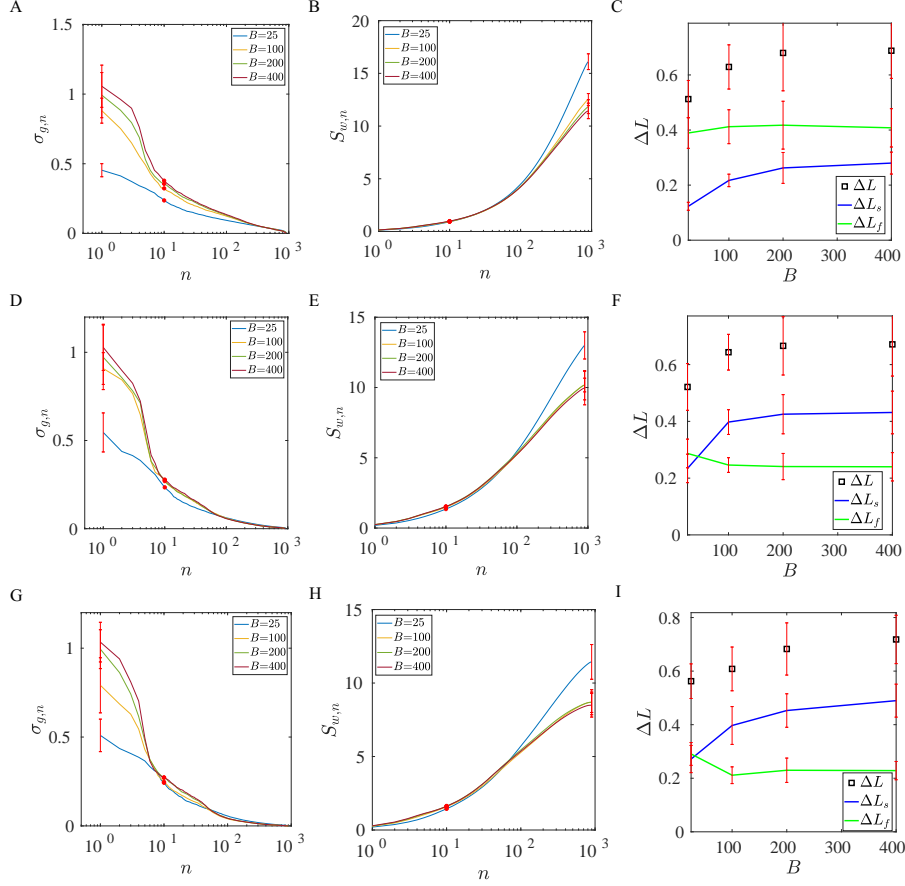


Fig. S8: The effects of changing batch size B in a multilayer fully connected network. Each row represents a hidden layer: (A-C), (D-F), and (G-I) show the sharpness spectrum $\sigma_{g,n}$, the accumulative weight variation $S_{w,n} = \sum_{i=1}^n \sigma_{w,i}$, and the generalization gap (ΔL) and the contributions from the sharp and flat directions (ΔL_s and ΔL_f), for hidden layer 1, 2, and 3, respectively.

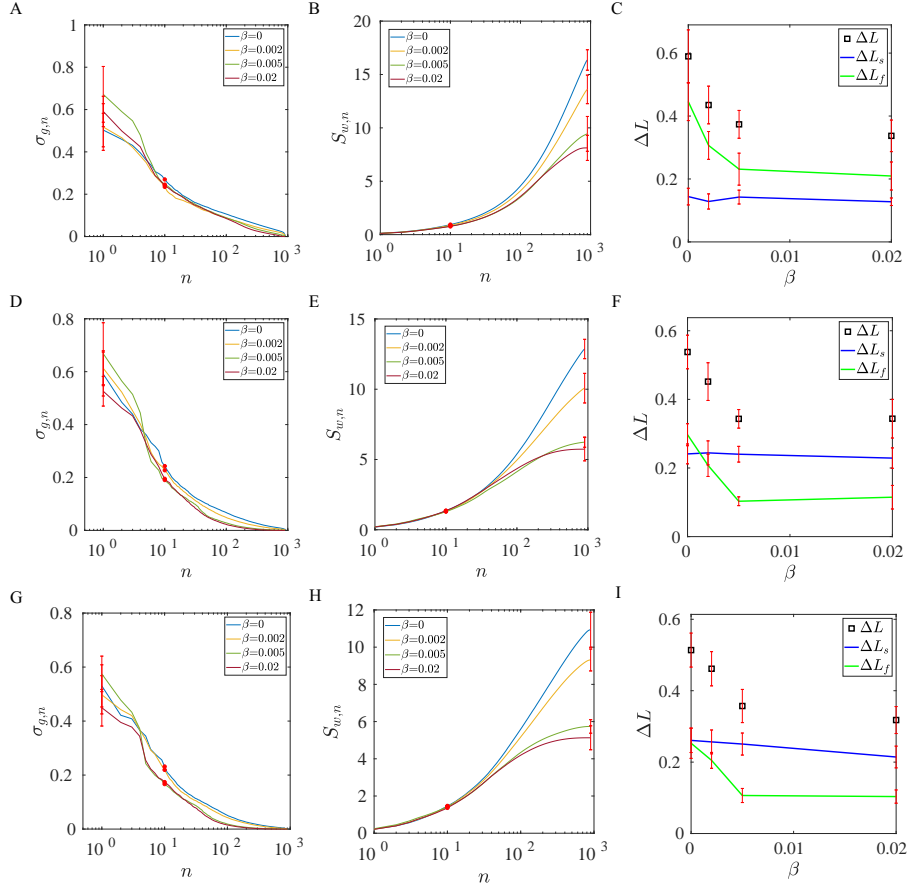


Fig. S9: The effects of changing weight decay rate β in a multilayer fully connected network. Each row represents a hidden layer: (A-C), (D-F), and (G-I) show the sharpness spectrum $\sigma_{g,n}$, the accumulative weight variation $S_{w,n} = \sum_{i=1}^n \sigma_{w,i}$, and the generalization gap (ΔL) and the contributions from the sharp and flat directions (ΔL_s and ΔL_f), for hidden layer 1, 2, and 3, respectively.

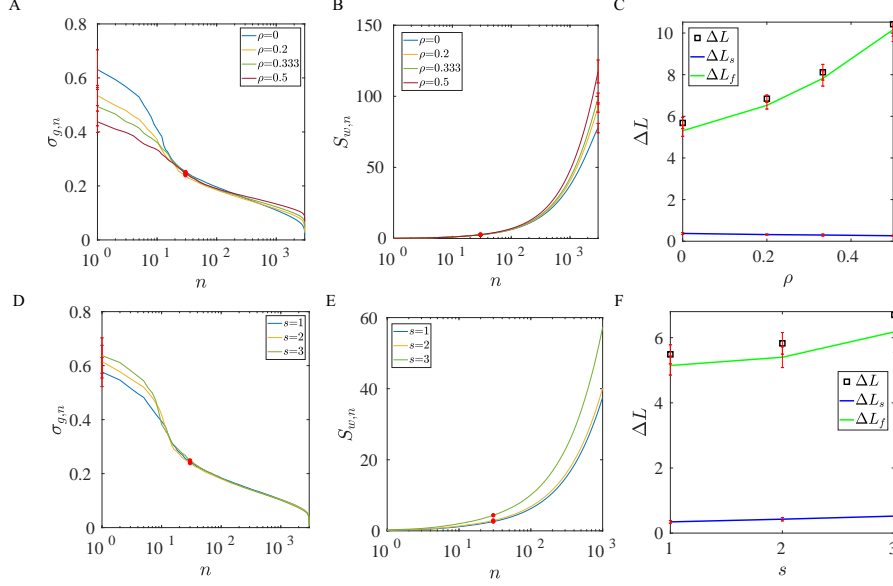


Fig. S10: Results for a FCL in a CNN trained with the CIFAR-10 dataset. (A-C) and (D-F) show the sharpness spectrum $\sigma_{g,n}$, the accumulative size $S_{w,n} = \sum_{i=1}^n \sigma_{w,i}$ for different s and ρ , and the generalization gap (ΔL) and the contributions from the sharp and flat directions (ΔL_s and ΔL_f), respectively.

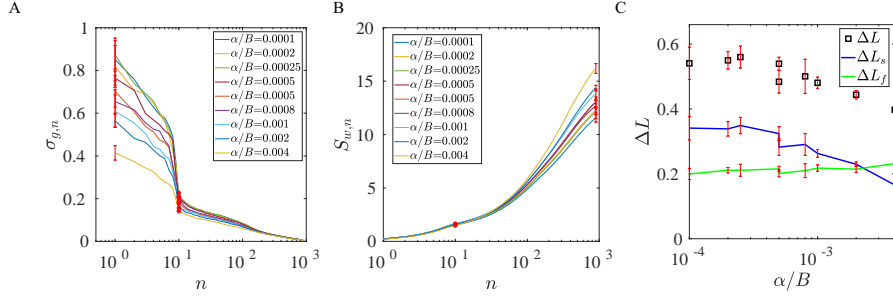


Fig. S11: The effects of changing both learning rate α and batch size B ($B = [25, 100, 200]$, $\alpha = [0.02, 0.05, 0.1]$). (A) The sharpness spectrum $\sigma_{g,n}$ for different values of α/B . (B) The accumulative size $S_{w,n} = \sum_{i=1}^n \sigma_{w,i}$ for different values of α/B . (C) The generalization gap (ΔL) and its contributions from the sharp and flat directions (ΔL_s and ΔL_f) versus α/B .